Electronic Supplementary Information (ESI)

Thermoswitchable on-chip microsupercapacitors: One potential self-protection solution for electronic devices

Panpan Zhang,‡[a,e] Jinhui Wang,‡[b,c] Wenbo Sheng,‡[d,e] Faxing Wang,[a,e] Jian Zhang,[a,e] Feng Zhu,[b,c] Xiaodong Zhuang,*[a,e] Rainer Jordan,[d,e] Oliver G. Schmidt[b,c,e] and Xinliang Feng*[a,e]

[a] Chair for Molecular Functional Materials, Department of Chemistry and Food Chemistry, School of Science, Technische Universität Dresden, Mommsenstr. 4, 01069 Dresden, Germany. E-mail: xiaodong.zhuang@tu-dresden.de; xinliang.feng@tu-dresden.de

[b] Material Systems for Nanoelectronics, Chemnitz University of Technology, Reichenhainer Str. 70, 09107 Chemnitz, Germany.

[c] Institute for Integrative Nanosciences, IFW Dresden, 01069 Dresden, Germany.

[d] Chair for Macromolecular Chemistry, Department of Chemistry and Food Chemistry, School of Science, Technische Universität Dresden, Mommsenstr. 4, 01069 Dresden, Germany.

[e] Center for Advancing Electronics Dresden (cfaed), Technische Universität Dresden, 01062 Dresden, Germany.

Experimental Section

Materials. *N*-isopropylacrylamide (NIPAAm, recrystallized in hexane), methylcellulose (MC, DS is 1.6), 3,4-ethylenedioxythiophene (EDOT), sodium dodecyl sulfate (SDS), H_2SO_4, LiCl, polyvinyl alcohol (PVA, molecular weight: 85,000-124,000), ammonium persulfate (APS), dimethylsulfoxide (DMSO) and *N,N,N',N'*-tetramethylethylenediamine were purchased from Sigma Aldrich. All reagents were analytical grade.

Synthesis of poly(N-isopropylacrylamide)-g-methylcellulose (PNIPAAm/MC) copolymer. The PNIPAAm/MC graft copolymer was synthesized by a reported method with minor modification.[1] First, NIPAAm was grafted to methylcellulose by using APS as initiator and *N,N,N',N'*-tetramethylethylenediamine as accelerator. Before starting the reaction, MC (100 mg) was dissolved in distilled water (5 mL) at 5 ^oC overnight. Then, NIPAAm (6.2 mg), MC solution, 2.5 mL of distilled water and 1% of APS were added into a four-round-bottom flask. After magnetic stirring and degassing with argon for 30 min, 25 μL of *N,N,N',N'*-tetramethylethylenediamine was added. The reaction was carried out at room temperature for 8 h under argon. Finally, as-produced PNIPAAm/MC graft copolymer was dialyzed in deionized water for 5 days to remove possible unreacted monomers and impurities. The transition temperature of sol-gel process of graft copolymer was carried out by differential scanning calorimetry (DSC). Gel permeation chromatography (GPC) data show that the weight-average molecular weight of PNIPAAm/MC is 4.22×10^6 g mol^{-1} and the molecular weight distribution is 1.52 (Fig. S39).

Device fabrication. Standard photolithography lift-off protocol was used to fabricate in-plane microsupercapacitors (MSCs). Photoresist AZ5214E was spun coated at 6000 rpm for 60 s over the cleaned Si/SiO_2 or polyimide (PI) substrates. Photoresist coated substrates were soft baked to remove the solvent at 90 ^oC for 4 min. The lithographic exposure was performed using mask-less aligner (Heidelberg PG 501, Germany) to establish the interdigital patterns. After this, hard baking at 120 ^oC for 2 min and flood exposure for 30 s were performed to make part

of photoresist cross-linked. Then, the treated substrates were developed in AZ726 MIF developer solution for 1 min which resulted in the formation of patterns on the photoresist layer. After plasma cleaning, metallic layers of 30 nm Au/10 nm Cr were deposited by e-beam evaporator (Edwards auto 500 FL500, England) over the patterned photoresist layer. Finally, the photoresist layer was lifted off in hot DMSO and thus patterned interdigital Au/Cr was achieved.

EDOT was electrochemically polymerized on Au electrodes in a standard three-electrode system using a patterned interdigital Au/Cr electrode as the working electrode, a Pt wire as the counter electrode, and Ag/AgCl (saturated KCl) as a reference electrode. The electrolyte solution contained 10 mM of EDOT, 10 mM of SDS, and 1 M of H_2SO_4. A constant anodic potential of 0.9 V was applied for 3 min during the process. Then the interdigital poly(3,4-ethylenedioxythiophene) (PEDOT)/Au/Cr electrode was washed with deionized water and air-dried at room temperature.

The polypyrrole (PPy) electrodes were also prepared using an electrochemical plating method. Anodic polymerization of pyrrole monomers on the patterned interdigital Au/Cr electrode was conducted at a constant potential of 0.8 V in the 0.05 M $LiClO_4$ and 0.05 M pyrrole monomers. After the polymerization, the electrodes were washed by both deionized water and ethanol several times to remove the by-products and impurities.

The electrolyte for thermoswitchable MSCs (TS-MSCs) was 0.1 M PNIPAAm/MC aqueous solution. In contrast, the PVA/LiCl gel electrolyte for conventional MSCs (C-MSCs) was prepared by mixing PVA powder (2.0 g) and LiCl (4.24 g) in 20 ml deionized water, and heated at 85 °C until the solution became clear.

Materials characterization. X-ray diffraction (XRD) patterns were recorded on an X-ray diffractometer (D/max-2200/PC, Rigaku) using Cu-Kα radiation (λ = 0.15418 nm) at 40 kV. The scanning electron microscopy (SEM) and the transmission electron microscopy (TEM) images were recorded on a field emission scanning electron microscope (FESEM, Zeiss Gemini

500) and a high-resolution transmission electron microscope (HRTEM, JEM-2100, JEOL, Japan), respectively. Raman analysis was performed by using a Raman spec-trometer (Renishaw inVia, 532 nm) at room temperature. The X-ray photoelectron spectroscopy (XPS) spectra were acquired using a Kratos Axis UltraDLD spectrometer (Kratos Analytical-A Shimadzu Group Company) with a monochromatic Al-Kα source (1486.6 eV).

Electrochemical measurement. A standard three-electrode system was fabricated using the PEDOT deposited on polyethylene terephthalate (PET, coated with 30 nm Au/10 nm Cr) film as the working electrode, a Pt wire as the counter electrode, Ag/AgCl (saturated KCl) as a reference electrode, 0.1 M PNIPAAm/MC/LiCl aqueous solution as the electrolyte. The electrochemical performance was carried out based on a CHI 750E electrochemical workstation. Cyclic voltammetric (CV) studies were examined at the scan rates of 100-2,000 V s^{-1}. Electrochemical impedance spectroscopy (EIS) was recorded in the frequency range of 10^{-1}-10^{5} Hz with 5 mV ac amplitude.

Calculations. The specific areal capacitances (C_A, mF cm^{-2}) based on the CV curves were calculated according to the following equation (1):

$$C_A = \frac{1}{2 \times S \times v \times (V_f - V_i)} \int_{V_i}^{V_f} I(V)dV \quad (1)$$

where C_A is the areal capacitance contributed by PEDOT, S is the total area of the electrodes (cm^2), v is the scan rate (V s^{-1}), V_f (final voltage) and V_i (initial voltage) are the integration potential limits of CV curves and $I(V)$ is the voltammetric current (in amperes). $\int_{V_i}^{V_f} I(V)dV$ represents the integral areas of CV curves.

The specific areal (C_A, mF cm^{-2}) and volumetric capacitances (C_V, F m^{-3}) were calculated from galvanostatic charge–discharge (GCD) curves by equation (2) and (3):

$$C_A = \frac{I}{S} \times \frac{t}{v} \quad (2)$$

$$C_V = \frac{C_A}{d} \tag{3}$$

where I/S is the current density (mA cm^{-2}) and t is the discharge time (s). v is the voltage range (0.8 V for this device) and d is the thickness of active materials.

The areal energy densities (E_A, Wh cm^{-2}) and power densities (P_A, W cm^{-2}) were calculated from equations (4) and (5), while the volumetric energy densities (E_V, Wh cm^{-3}) and power densities (P_V, W cm^{-3}) were calculated from equations (6) and (7):

$$E_A = \frac{1}{2} \times C_A \times \frac{(\Delta V)^2}{3{,}600} \tag{4}$$

$$P_A = \frac{E_A}{\Delta t} \times 3{,}600 \tag{5}$$

$$E_V = \frac{1}{2} \times C_V \times \frac{(\Delta V)^2}{3{,}600} \tag{6}$$

$$P_V = \frac{E_V}{\Delta t} \times 3{,}600 \tag{7}$$

where ΔV is the discharge voltage range (0.8 V) and Δt is discharge time (s).

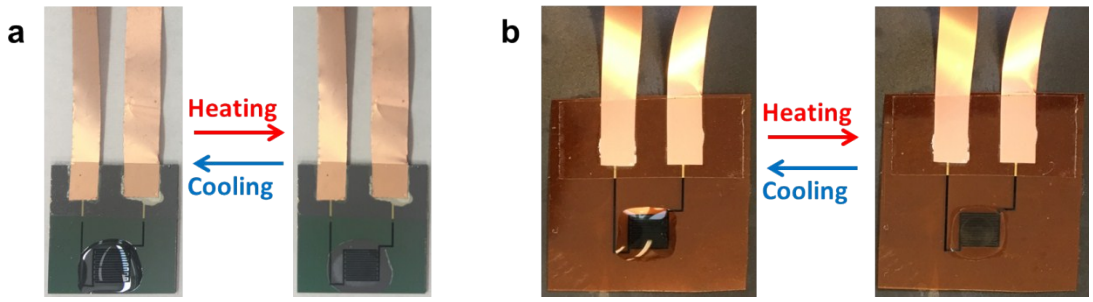

Fig. S1 Digital photos of single TS-MSCs upon heating and cooling on (a) a rigid Si/SiO_2 wafer and (b) a flexible PI film.

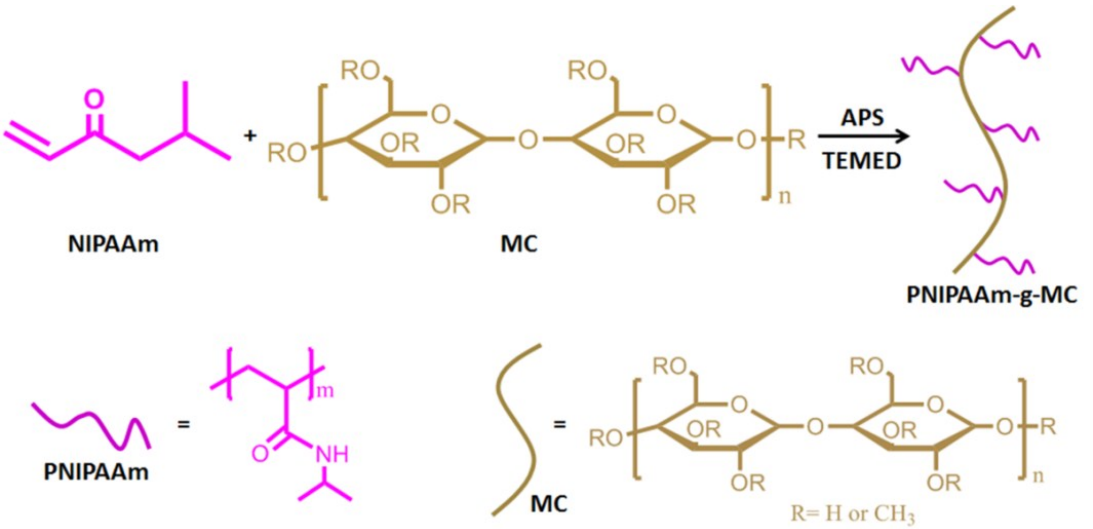

Fig. S2 Synthesis route toward thermoresponsive graft copolymer (PNIPAAm/MC).

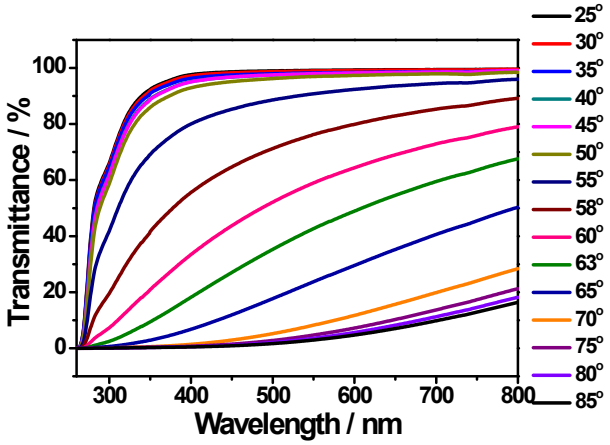

Fig. S3 In-situ transmittance measurement of PNIPAAm/MC solution in the 300–800 nm window upon heating from 25 to 85 °C.

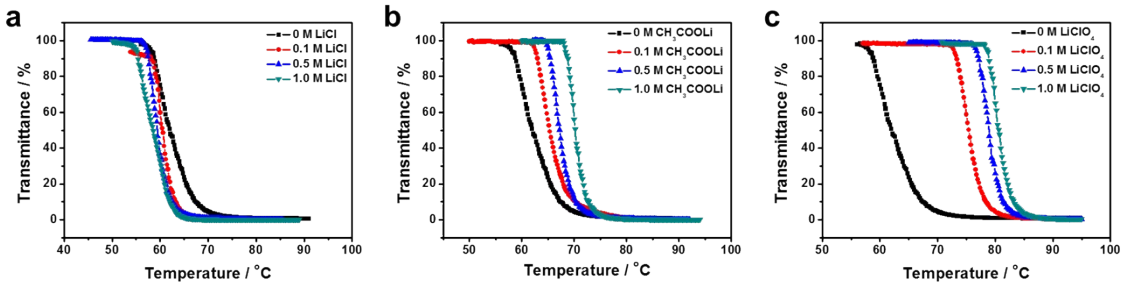

Fig. S4 Temperature-dependent transmittances at 600 nm of the electrolytes of PNIPAAm/MC mixed with different lithium salts and concentrations: (a) lithium chloride, (b) lithium acetate, and (c) lithium perchlorate.

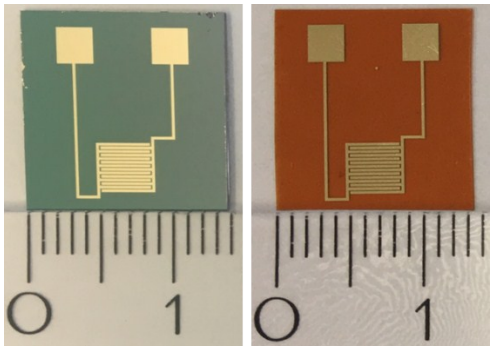

Fig. S5 Digital photographs of patterned interdigital electrodes on silicon wafer (left) and PI film (right).

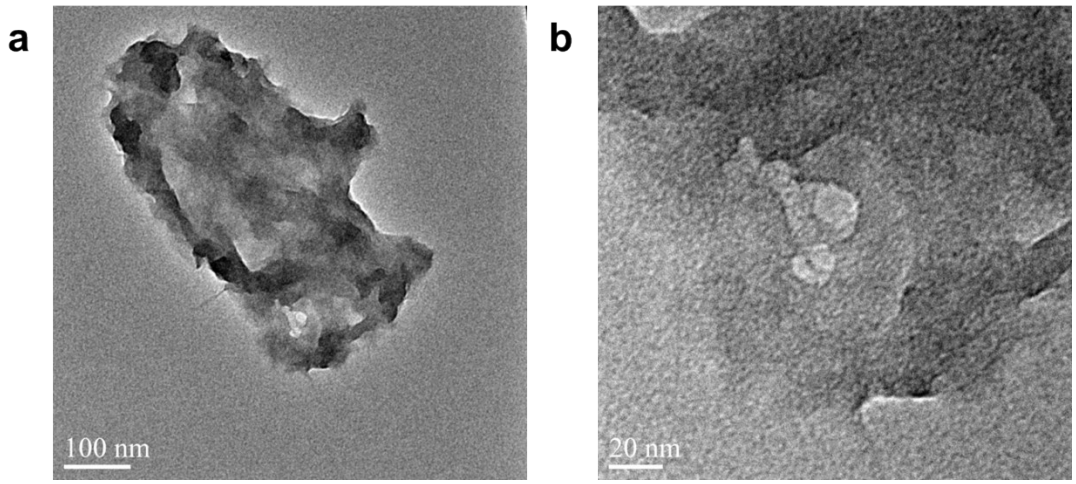

Fig. S6 HRTEM images of PEDOT with different magnifications.

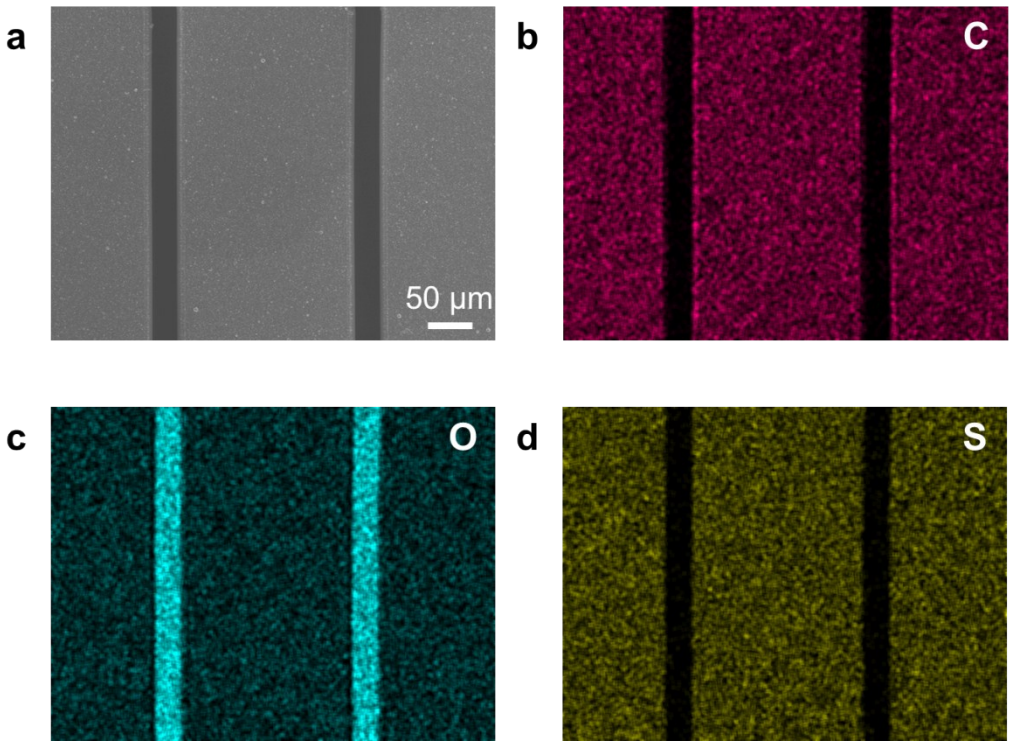

Fig. S7 Top-view SEM image of PEDOT/Au interdigital finger electrodes and corresponding energy-dispersive spectroscopy (EDS) elemental mapping analysis.

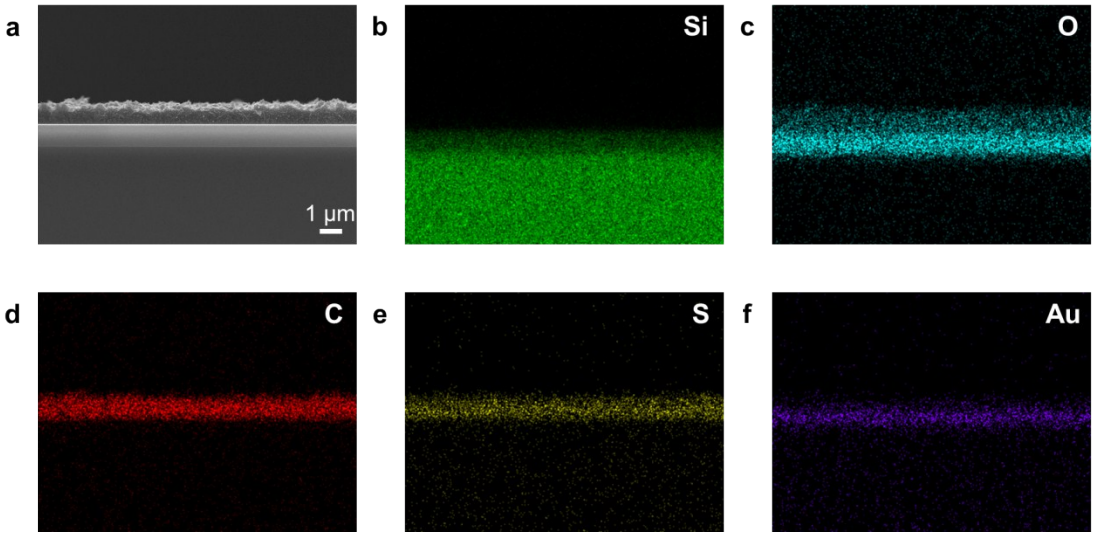

Fig. S8 Side-view SEM image of PEDOT/Au/SiO_2/Si electrode with layered structure, corresponding EDS elemental mapping analysis and spectrum of Si, O, C, S, Au elements, respectively.

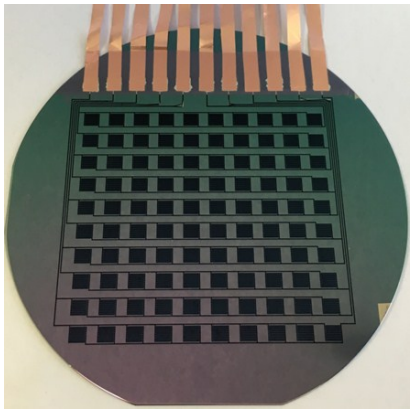

Fig. S9 Digital photograph of 100 TS-MSCs with 10 MSCs in parallel for each line and 10 lines in series on a 3-in Si wafer.

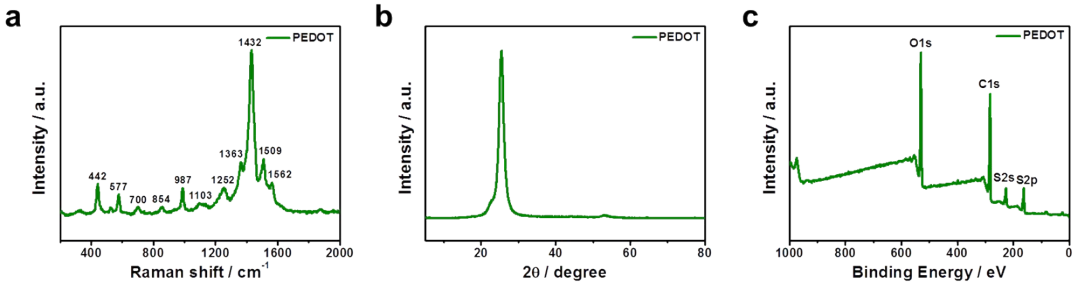

Fig. S10 Structure characterizations of PEDOT electrodes. (a) Raman spectrum, (b) XRD pattern, and (c) XPS spectrum.

Structural characterizations of the PEDOT film were studied by Raman spectroscopy, XRD pattern, and XPS spectrum. The main peaks at 1562 and 1509 cm^{-1} in the Raman spectrum can be assigned to the asymmetric stretching of $C_\alpha = C_\beta$, and the most intense peak at 1432 cm^{-1} corresponds to the stretching of $C_\alpha = C_\beta(-O)$, indicating high oxidation state of PEDOT.[2] The other characteristic peaks of PEDOT in Raman spectrum at 442 cm^{-1} (SO_2 bending), 577 cm^{-1}

(oxy-ethylene ring deformation), 700 cm^{-1} (symmetric C–S–C deformation), 987 cm^{-1} (C–C antisymmetrical stretching mode), 1103 cm^{-1} (C–O–C deformation), 1252 cm^{-1} (C_α–C_α interring stretching), and 1363 cm^{-1} (C_β–C_β interring stretching) are consistent with the previously reported data.[3-5] The XRD pattern of the PEDOT film reveals a characteristic peak (2θ) at approximately 26°, which can be attributed to the interpolymer chain stacking.[6] XPS spectrum shows the bands at 530.0, 283.0, 226.0, and 162.0 eV, which are associated with the characteristic peaks of O 1s, C 1s, S 2s, and S 2p, respectively, also confirming the formation of PEDOT and the doping of sulfate and bisulfate anions in PEDOT nanostructures.[7,8] Thus, the PEDOT layer was successfully formed through electrochemical deposition.

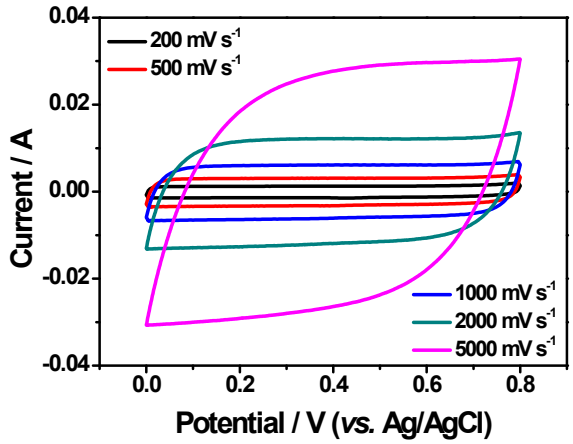

Fig. S11 CV curves of PET-supported PEDOT film at different scan rates in 0.1 M PNIPAAm/MC/LiCl aqueous solution at room temperature.

PEDOT as one of the most commonly used conductive polymers for supercapacitors can provide pseudocapacitance by fast p-doping and p-dedoping surface redox reactions and electrochemical double layer capacitance by electrostatic adsorption.[8,9] At low scan rates (<50 mV s^{-1}), the PEDOT usually displays rectangular shape with a broad redox peak in CV curves in conventional supercapacitors. However, in the current work, one of the advantages of the MSC is the fast rate capability, which can be operated at high scan rates ranging from 200 to 5000 mV s^{-1}. To be consistent with the PEDOT-based MSC, the three-electrode tests for the PEDOT electrode were also conducted at such high scan rates. At high sweep rates (>100 mV s^{-1}), the diffusional limitation of doping process in the PEDOT electrode leads to the disappearance of broad redox peak in the CV curves. In this case, the electrochemical double layer capacitance dominates the charge storage in PEDOT electrode and produces rectangular shape without showing redox peaks. This result is consistent with the previous reports on PEDOT electrode operated at high scan rates.[10-12]

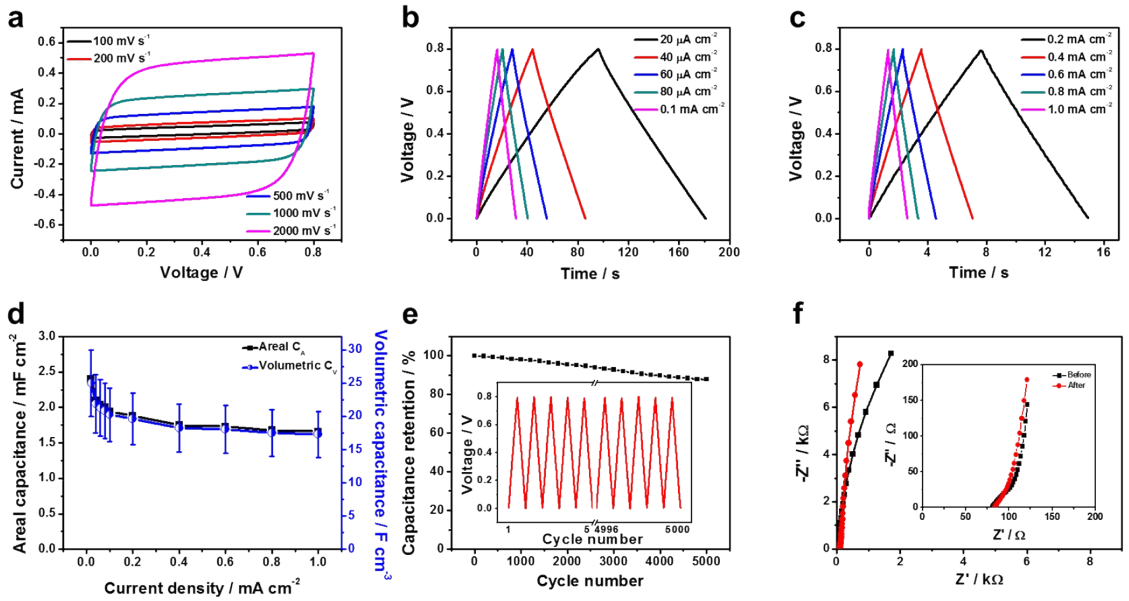

Fig. S12 Electrochemical performance of TS-MSC at room temperature: (a) CV curves at scan rates of 100–2000 mV s^{-1}, (b, c) GCD curves at current densities of 20–1000 μA cm^{-2}, (d) specific capacitances calculated from GCD curves as function of current densities, (e) cycling stability at a current density of 0.1 mA cm^{-2} (Inset shows the first and last five GCD curves), and (f) Nyquist plots of as-prepared TS-MSC before and after 5000 charge-discharge cycling measurement. Inset depicts an enlarged high-frequency region.

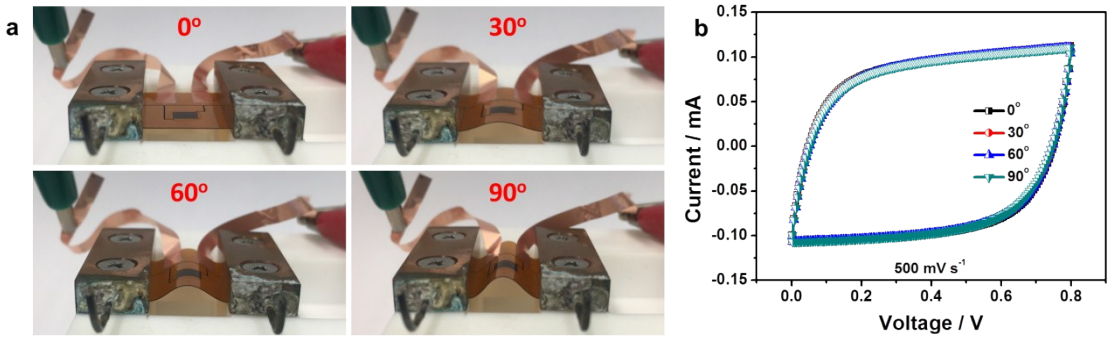

Fig. S13 The flexibility of TS-MSC on PI substrate. (a) Optical images of PI-supported TS-MSC bended with different angles. (b) CV curves of PI-supported TS-MSC bended with different angles at the scan rate of 500 mV s^{-1}.

The CV curves for the PI-supported TS-MSC were examined at a scan rate of 500 mV s^{-1} at four bending angles (0°, 30°, 60°, and 90°). No obvious changes were observed for the CV curves under different bending states, highlighting the good flexibility and electrochemical stability of the PI-supported MSC for flexible micro-devices.

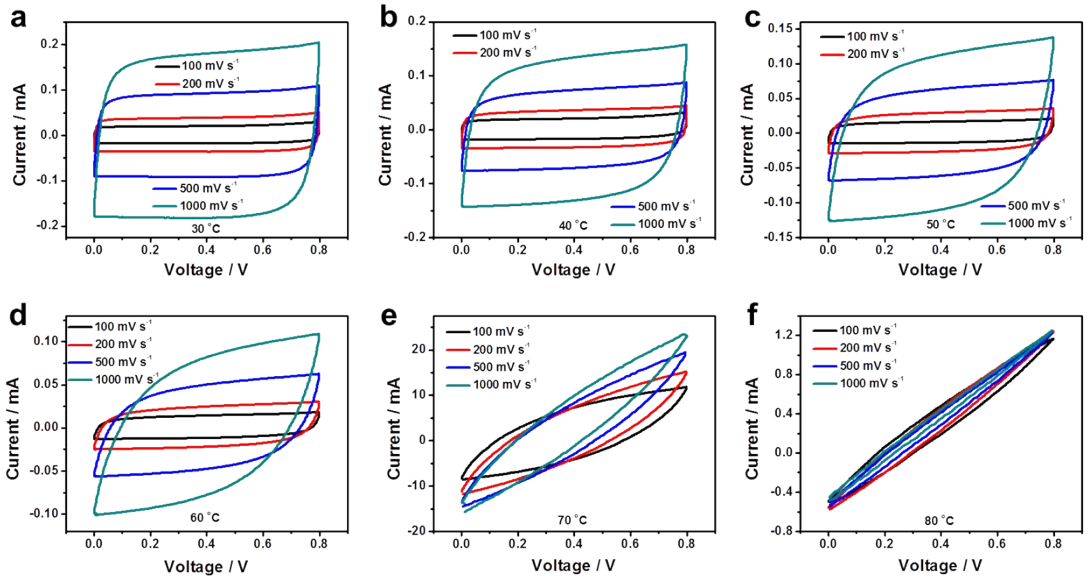

Fig. S14 CV curves of single TS-MSC at different scan rates varied from 100 to 1000 mV s^{-1} in the temperature range of 30-80 °C.

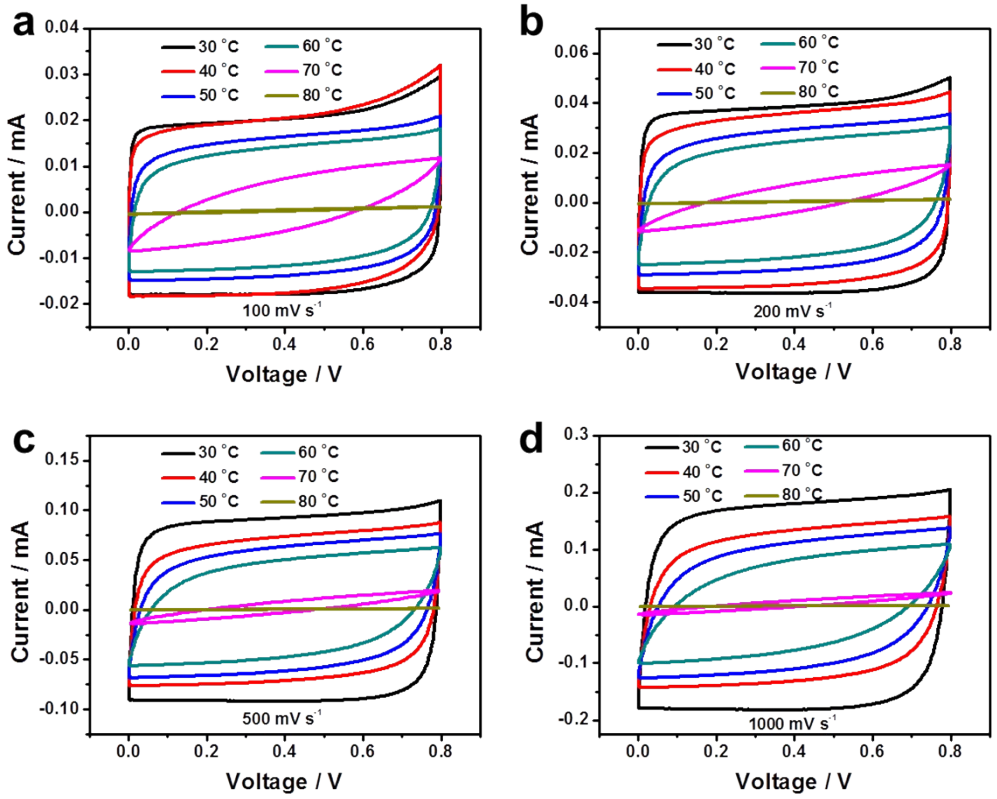

Fig. S15 Comparisons of CV curves of single TS-MSC at different scan rates varied from 100 to 1000 mV s^{-1} in the temperature range of 30-80 °C.

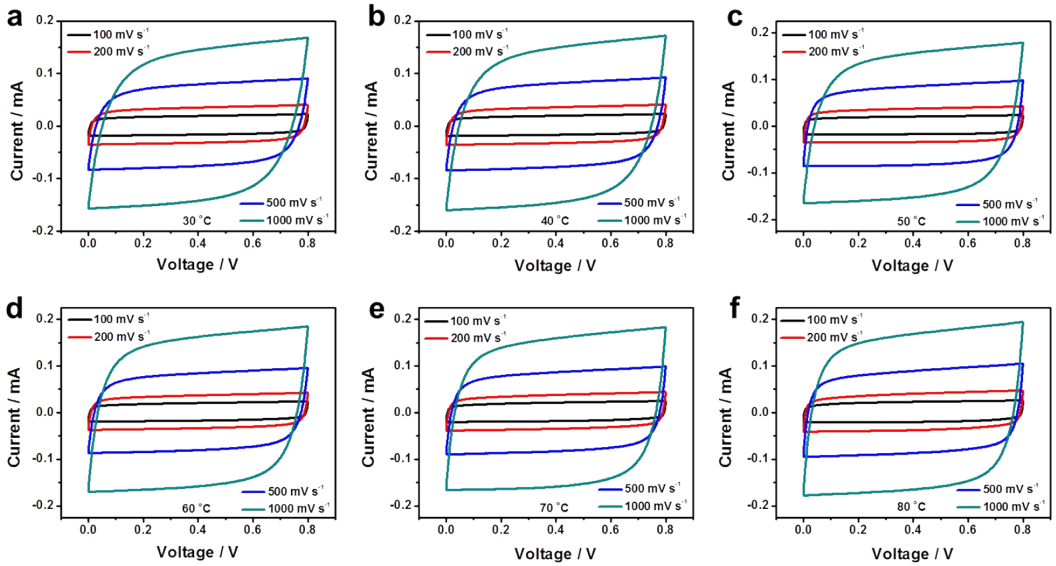

Fig. S16 CV curves of single C-MSC at different scan rates varied from 100 to 1000 mV s^{-1} in the temperature range of 30-80 °C.

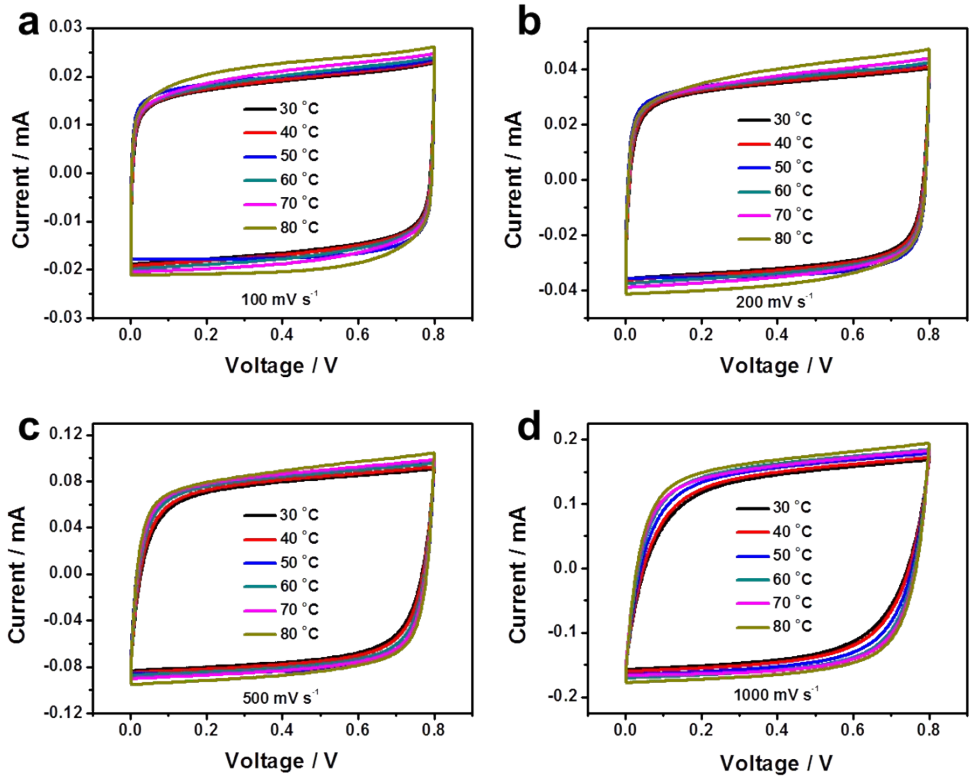

Fig. S17 Comparisons of CV curves of single C-MSC at different scan rates varied from 100 to 1000 mV s^{-1} in the temperature range of 30-80 °C.

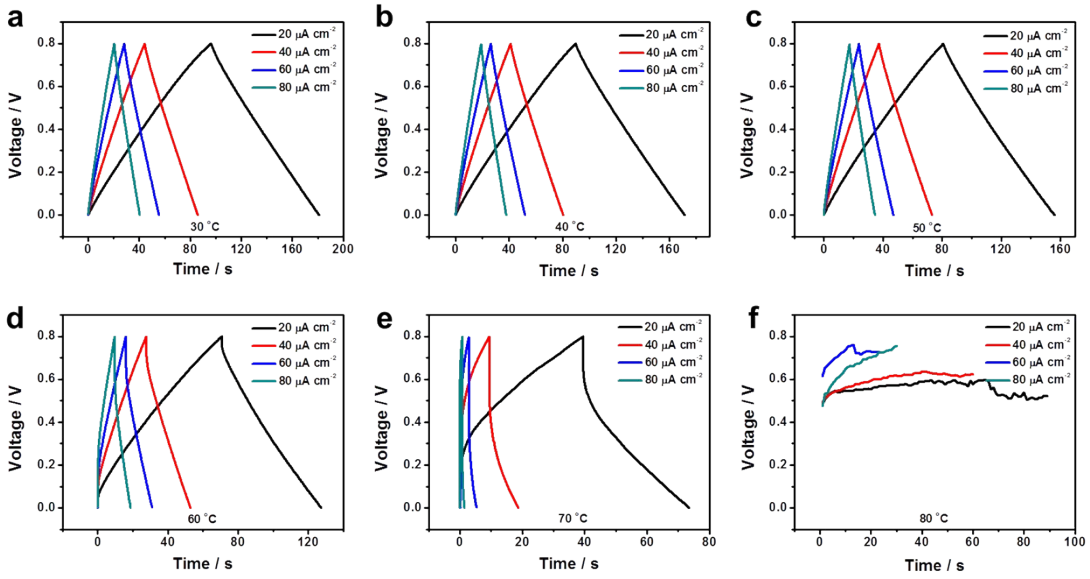

Fig. S18 GCD curves of single TS-MSC at different current densities varied from 20 to 80 μA cm^{-2} in the temperature range of 30-80 °C.

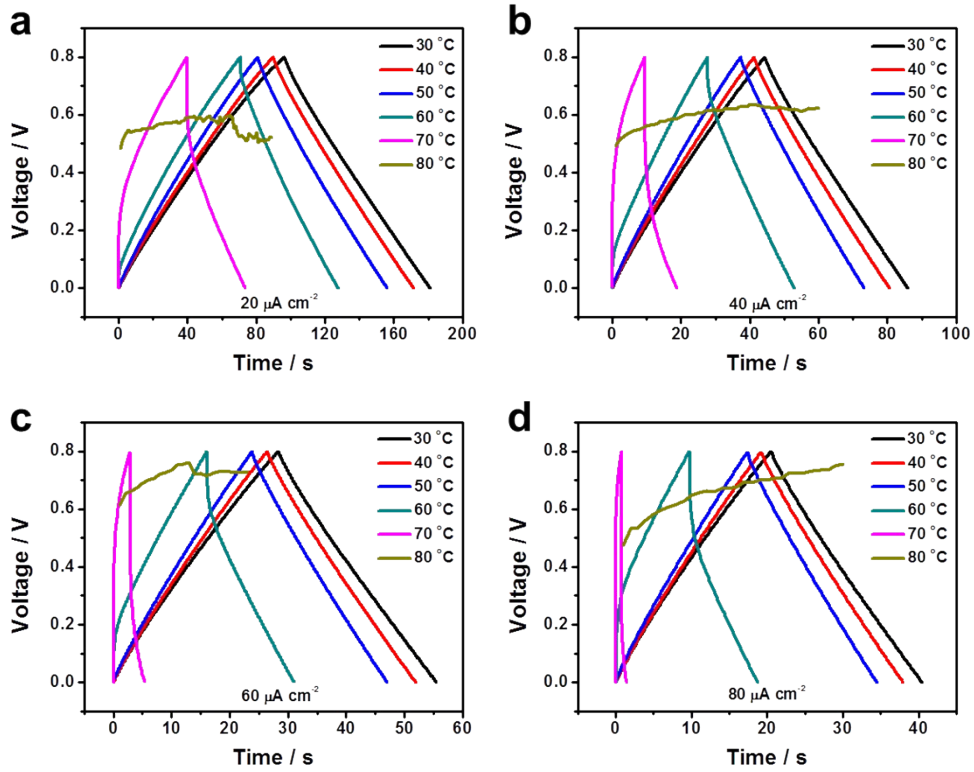

Fig. S19 Comparisons of GCD curves of single TS-MSC at different current densities varied from 20 to 80 μA cm^{-2} in the temperature range of 30-80 °C.

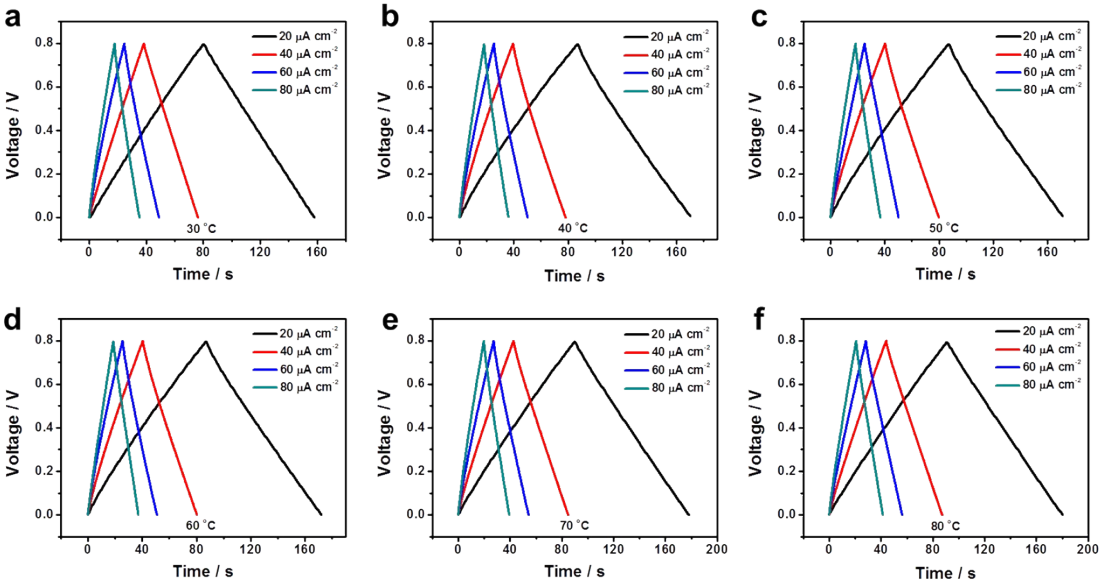

Fig. S20 GCD curves of single C-MSC at different current densities varied from 20 to 80 μA cm^{-2} in the temperature range of 30-80 °C.

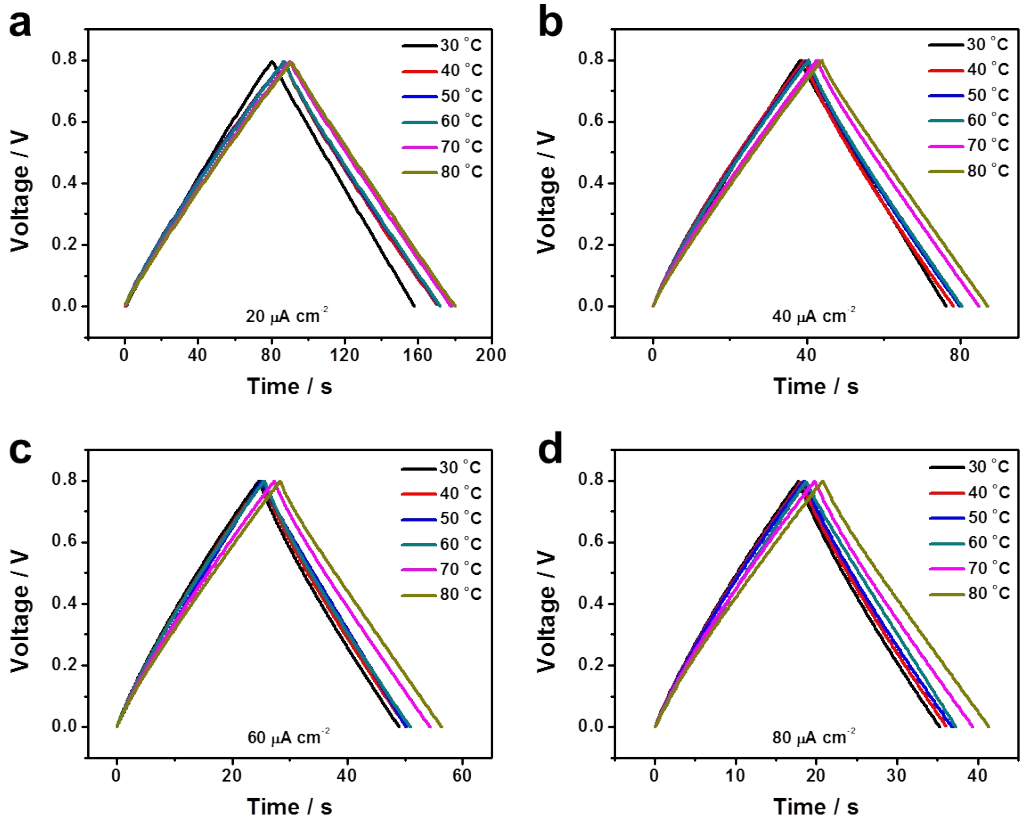

Fig. S21 Comparisons of GCD curves of single C-MSC at different current densities varied from 20 to 80 μA cm^{-2} in the temperature range of 30-80 °C.

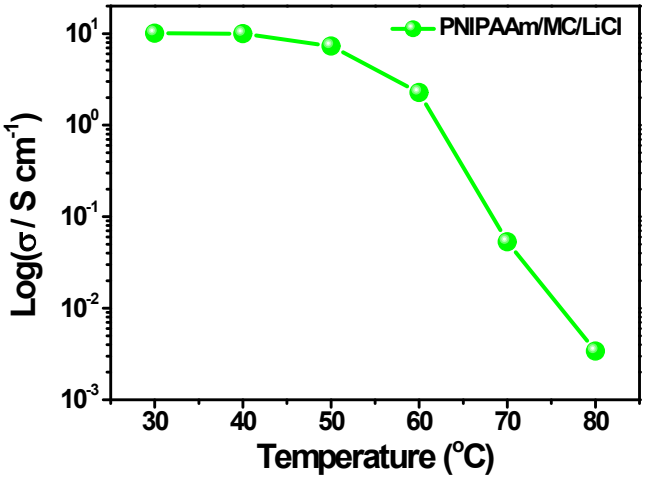

Fig. S22 Log (ionic conductivities) *vs* temperature plots for the thermoresponsive PNIPAAm/MC/LiCl electrolyte on increasing the temperature from 30 to 80 °C.

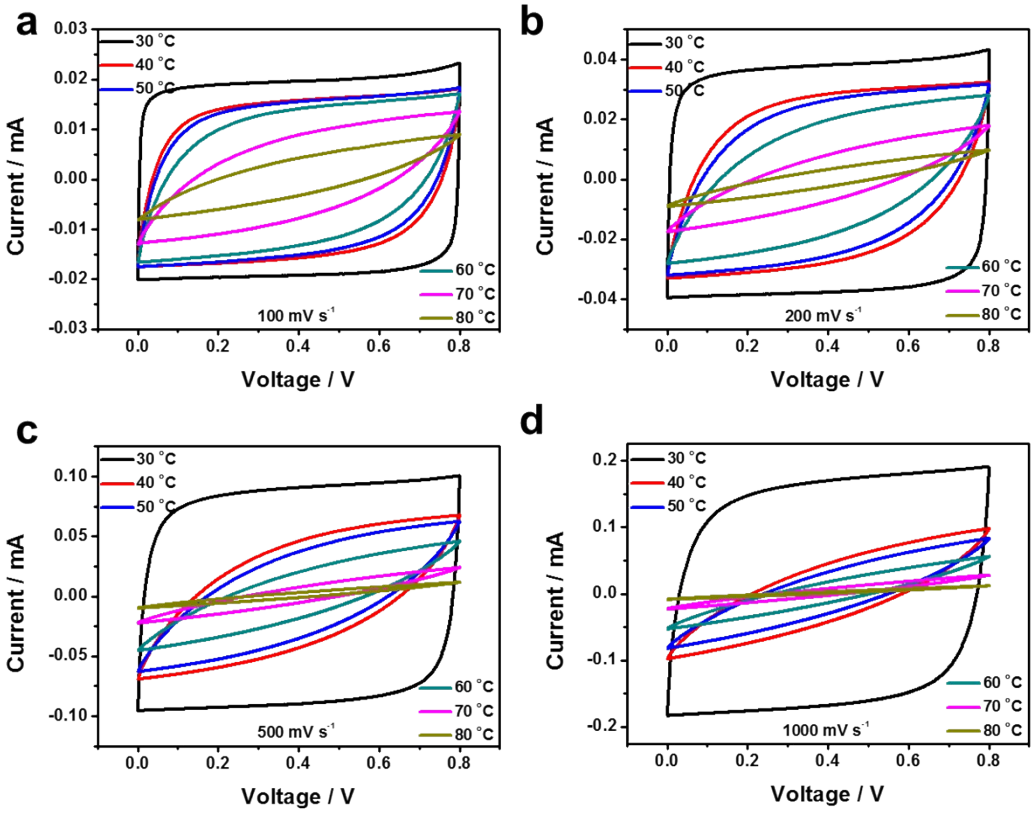

Fig. S23 Comparisons of CV curves of single TS-MSC-CH_3COOLi (0.1 M) at different scan rates varied from 100 to 1000 mV s^{-1} in the temperature range of 30-80 °C.

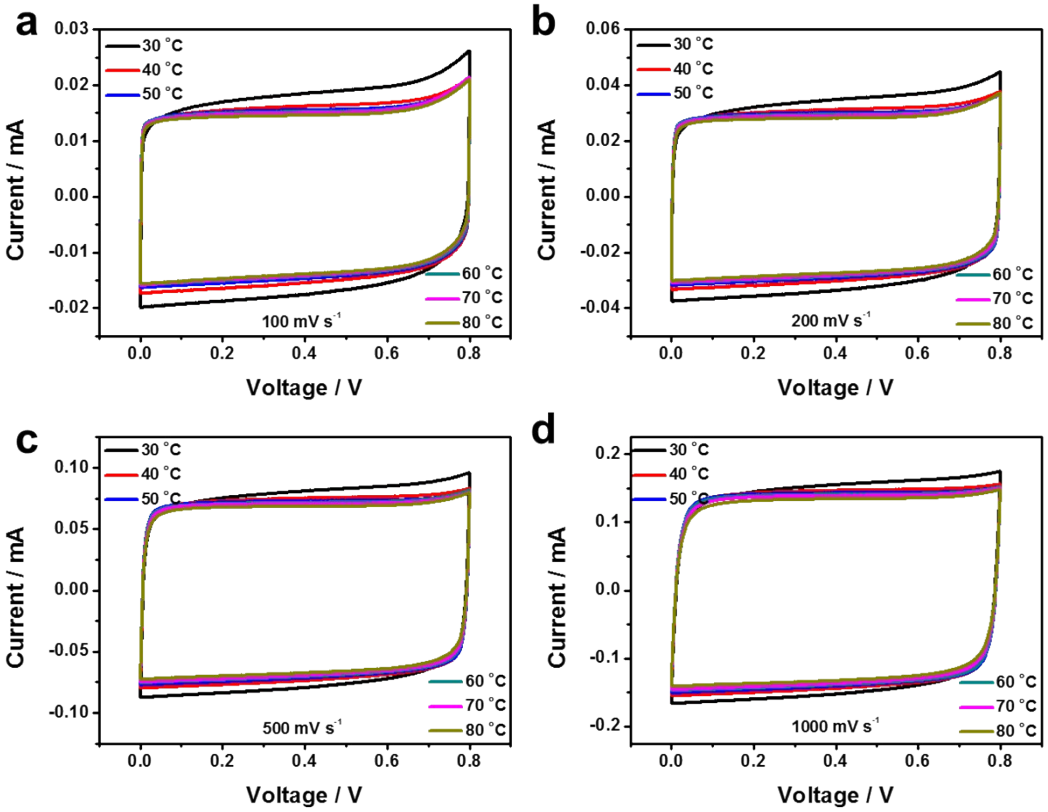

Fig. S24 Comparisons of CV curves of single TS-MSC-$LiClO_4$ (0.1 M) at different scan rates varied from 100 to 1000 mV s^{-1} in the temperature range of 30-80 °C.

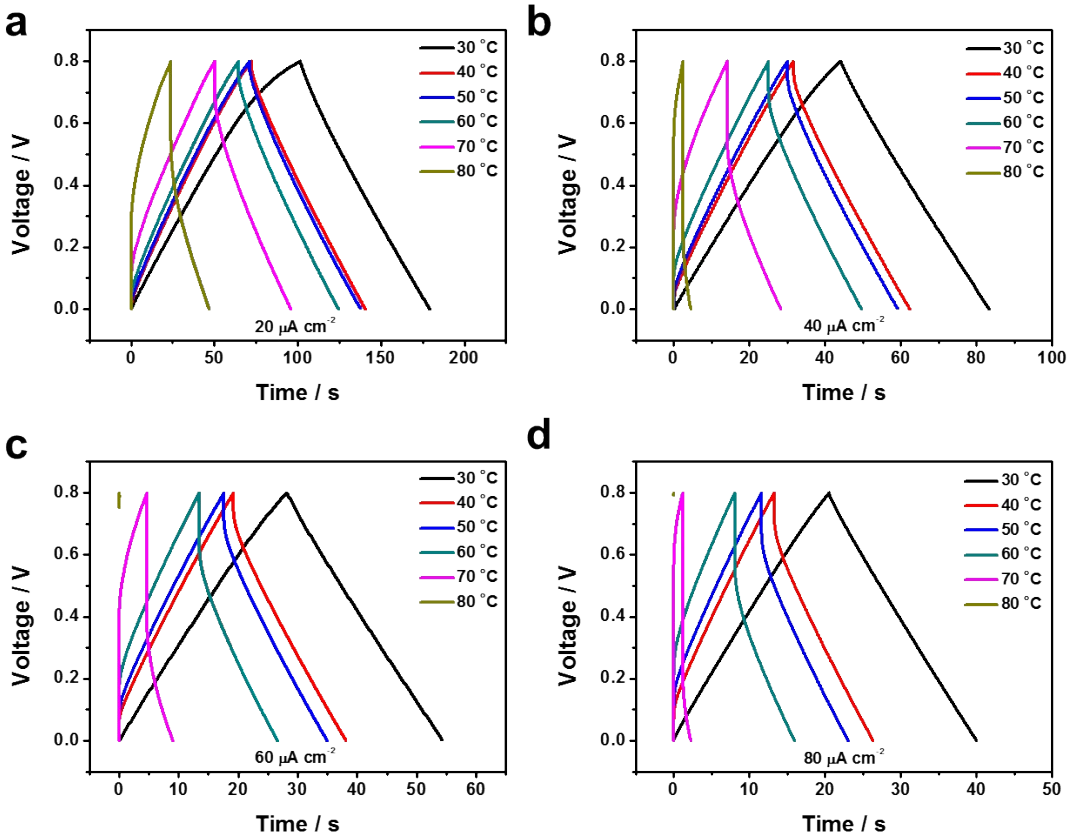

Fig. S25 Comparisons of GCD curves of single TS-MSC-CH_3COOLi (0.1 M) at different current densities varied from 20 to 80 μA cm^{-2} in the temperature range of 30-80 °C.

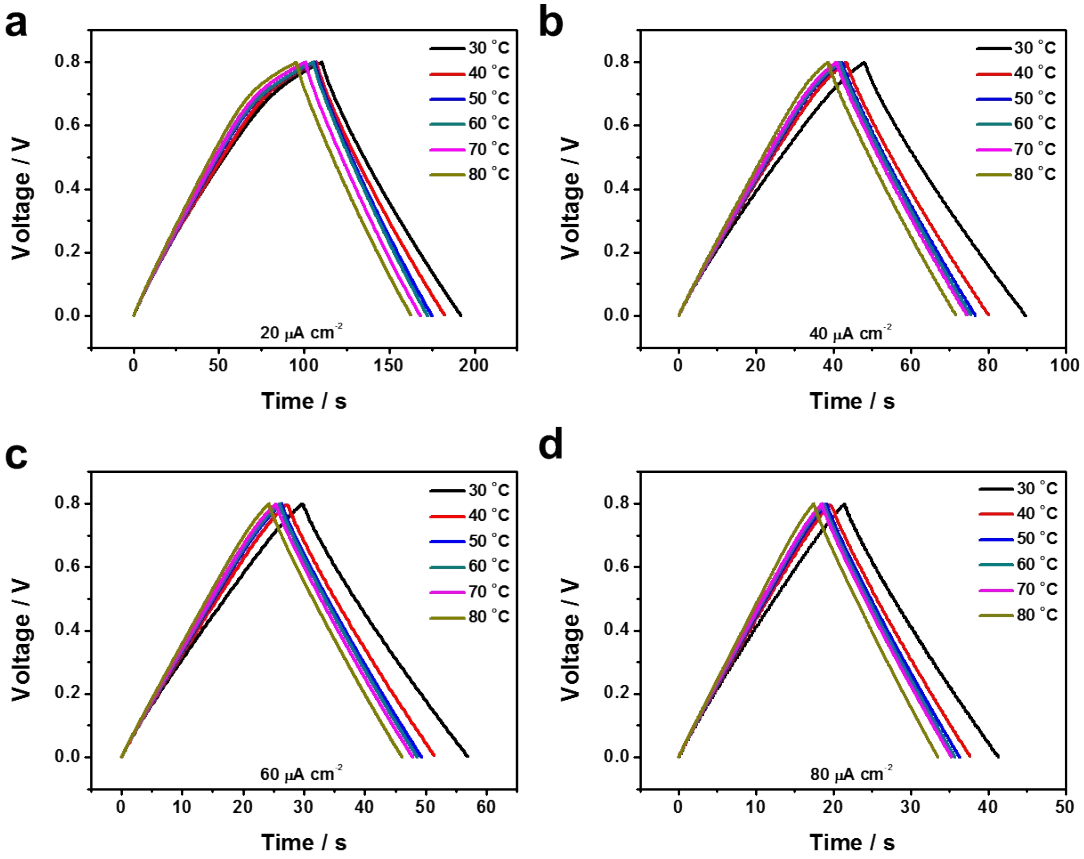

Fig. S26 Comparisons of GCD curves of single TS-MSC-$LiClO_4$ (0.1 M) at different current densities varied from 20 to 80 μA cm^{-2} in the temperature range of 30-80 °C.

In comparison, PEDOT-based in-plane MSCs with two different electrolytes of PNIPAAm/MC/CH_3COOLi and PNIPAAm/MC/$LiClO_4$ (denoted as TS-MSC-CH_3COOLi, TS-MSC-$LiClO_4$) were fabricated to address the effect of electrolyte anions on the thermoresponsive behavior. Obviously, the capacitance of TS-MSC-CH_3COOLi decreased gradually upon increasing the temperature from 30 to 80 °C but still exhibited a low areal capacitance of 155 μF cm^{-2} (81.5% fading) at 80 °C (Fig. S23), while TS-MSC-$LiClO_4$ decreased only 16% up to 80 °C (Fig. S24). Moreover, GCD curves confirmed ineffective switch-off behavior of CH_3COO^- and ClO_4^- for thermal protection (Fig. S25 and S26), in accordance with the changes of the transmittances at 600 nm (Fig. S4b and c).

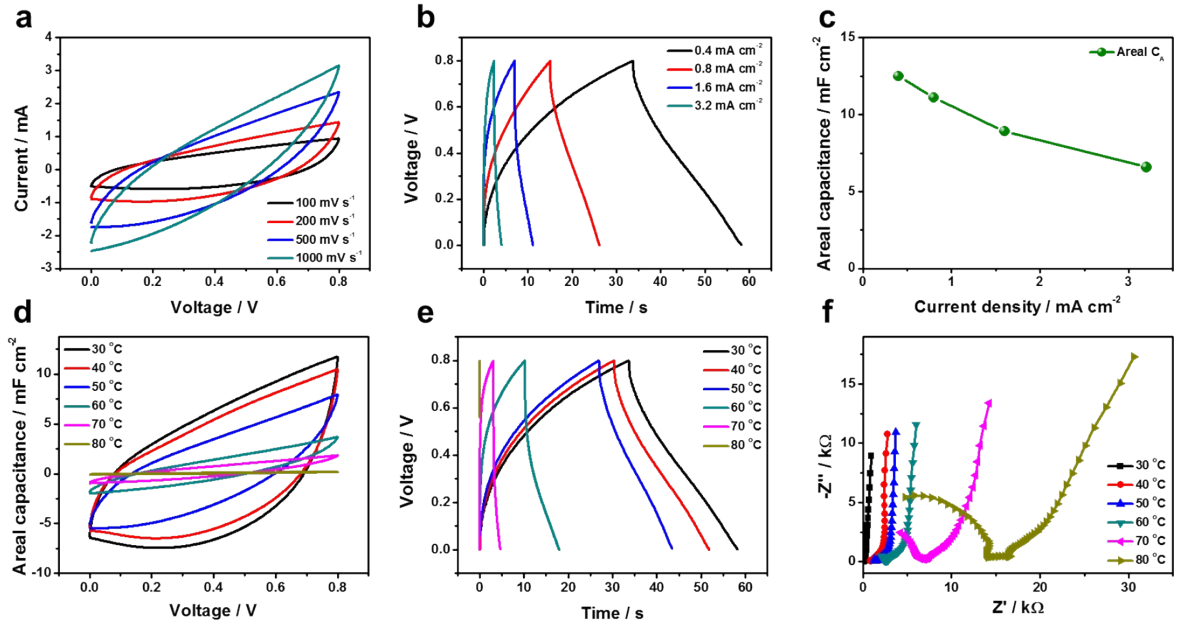

Fig. S27 Performance of TS-MSC based on PPy at room temperature: (a) CV curves at different scan rates from 100 to 1000 mV s^{-1}. (b) GCD curves at different current densities varied from 0.4 to 3.2 mA cm^{-2}. (c) Specific areal capacitances calculated from GCD curves as function of current densities. The thermoresponsive behavior of TS-MSCs based on PPy: (d) CV curves at a scan rate of 100 mV s^{-1}, (e) GCD curves at a current density of 0.4 mA cm^{-2} and (f) Nyquist plots of a TS-MSC based on PPy upon increasing the temperature from 30 to 80 °C.

Given that the thermoresponsive behavior mainly depends on the chemical and ionic conductive properties of the polymer electrolyte, versatile electrode materials can be also employed for the fabrication of thermoswitchable MSCs. For instance, we further constructed a polypyrrole (PPy)-based in-plane MSC with the same thermoresponsive electrolyte. Both of the CV and GCD curves show typical capacitive behavior (Fig. S27a-c). The areal capacitance calculated from the GCD curve at 0.4 mA cm^{-2} was 12.5 mF cm^{-2}, which can maintain up to 6.58 mF cm^{-2} at the current density of 3.2 mA cm^{-2}. Obviously, the specific areal capacitance deceased to zero upon increasing the temperature from 30 to 80 ^{o}C (Fig. S27d and e). Furthermore, the significant increase of EIS resistance indicated the inhibited migration of Li^{+} ions (Fig. S27f). The above results suggest the universal strategy for TS-MSCs.

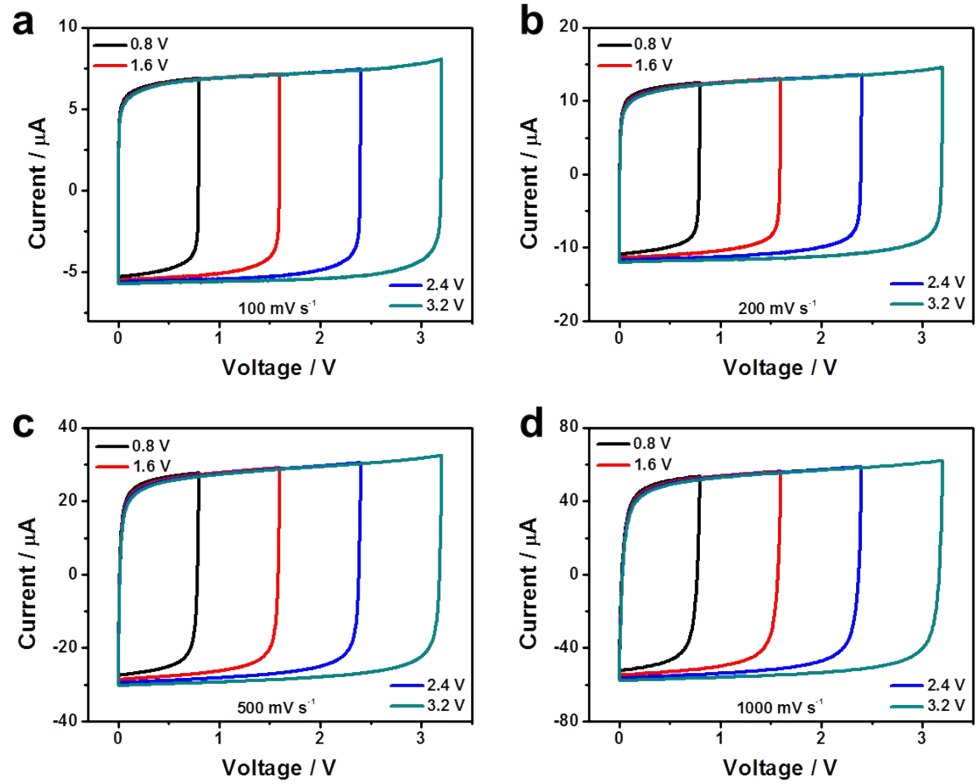

Fig. S28 CV curves of four TS-MSCs connected in series at different scan rates varied from 100 to 1000 mV s^{-1} at room temperature.

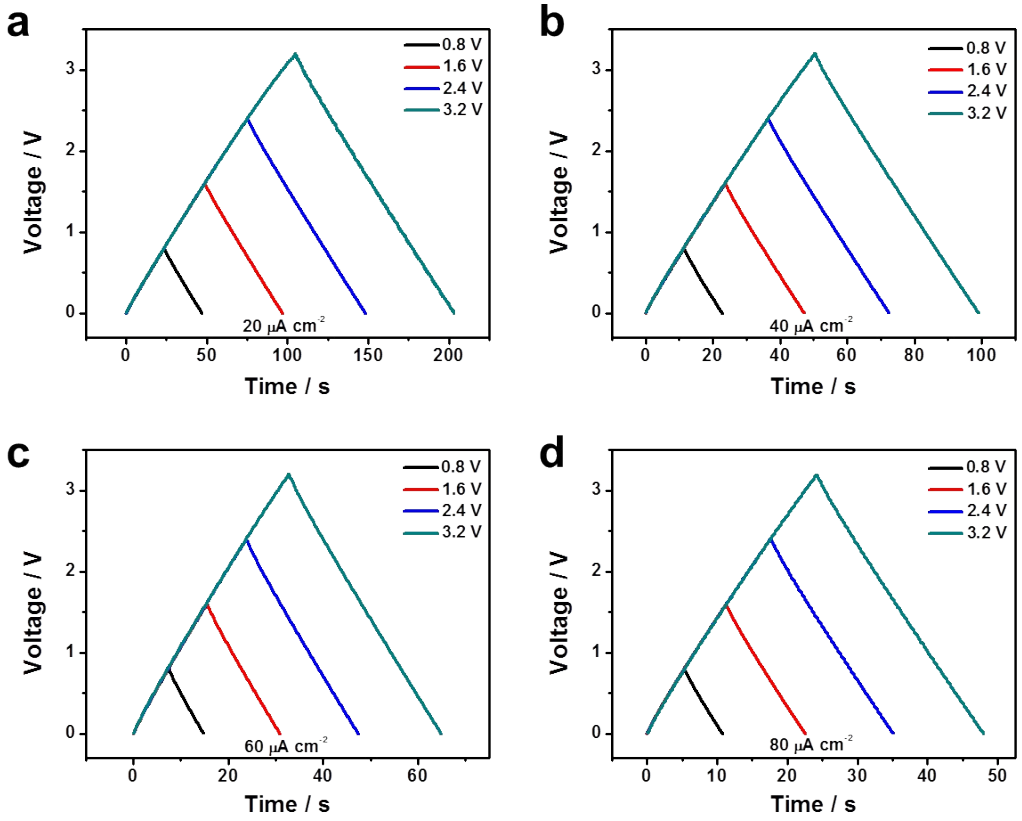

Fig. S29 GCD curves of four TS-MSCs connected in series at different current densities varied from 20 to 80 μA cm^{-2} at room temperature.

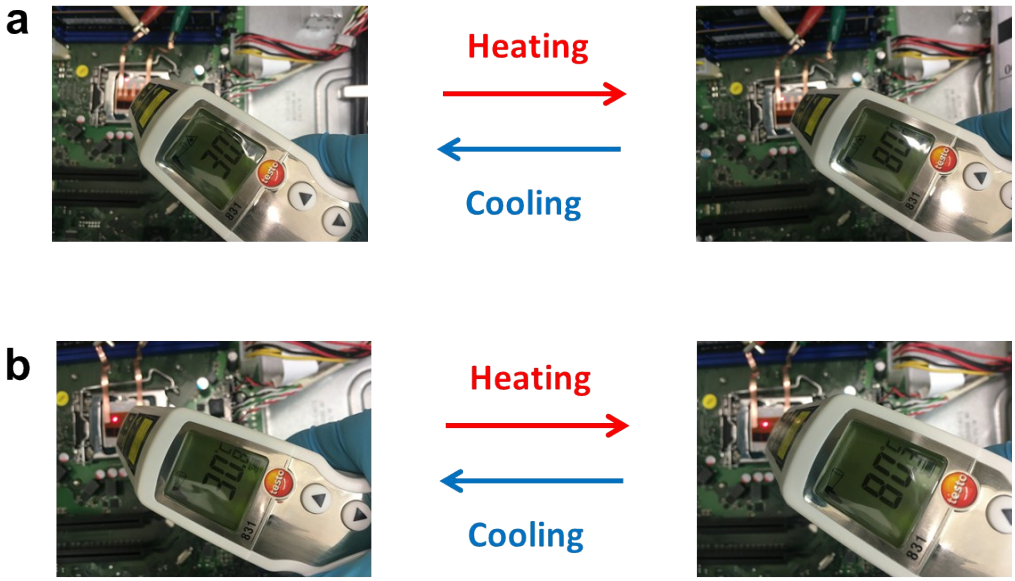

Fig. S30 (a, b) The non-contact infrared thermometer displayed the real-time temperatures of the CPU panel and TS-MSCs array corresponding to Fig. 5a and 5d, respectively.

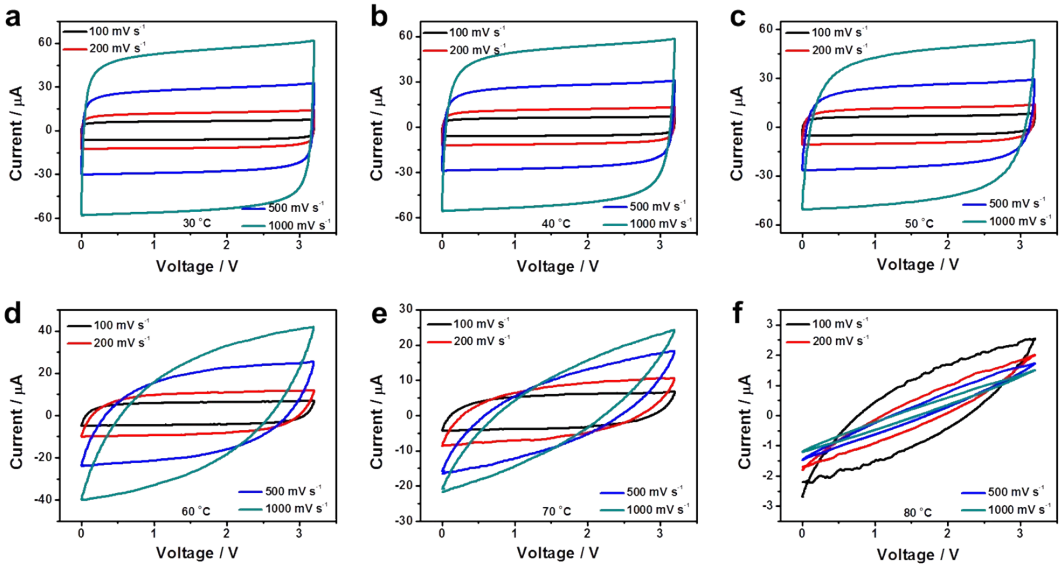

Fig. S31 CV curves of four TS-MSCs connected in series at different scan rates varied from 100 to 1000 mV s^{-1} in the temperature range of 30–80 °C.

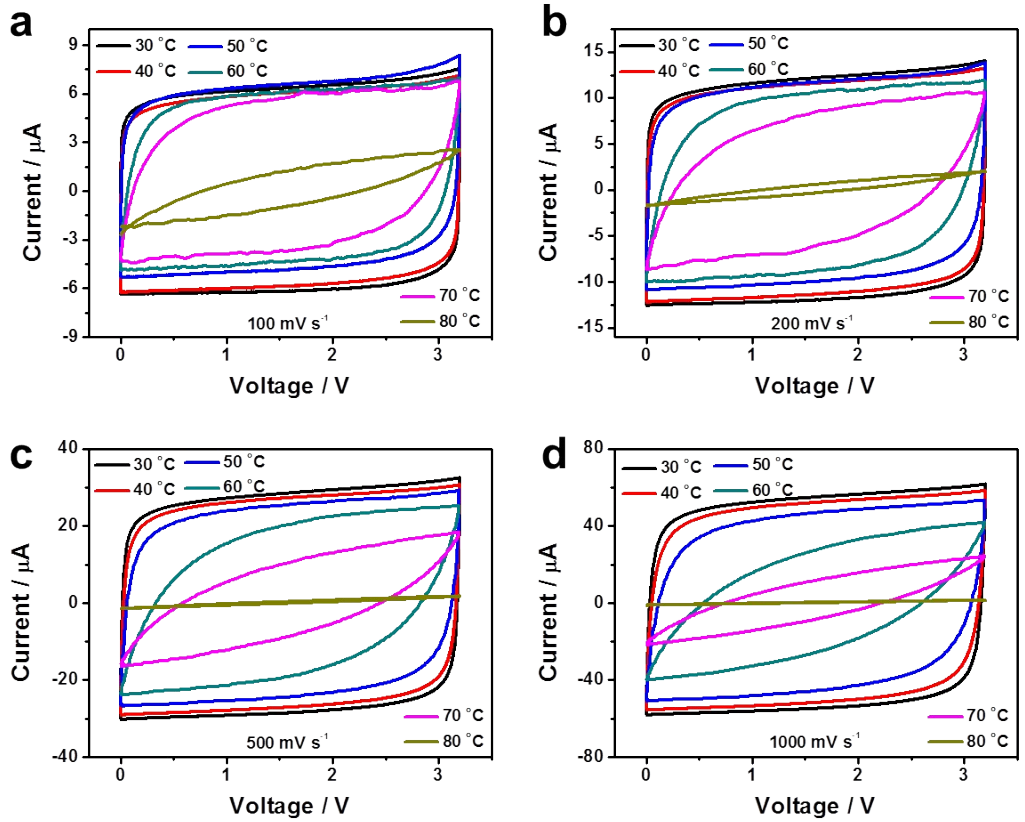

Fig. S32 Comparisons of CV curves of four TS-MSCs connected in series at different scan rates varied from 100 to 1000 mV s^{-1} in the temperature range of 30–80 °C.

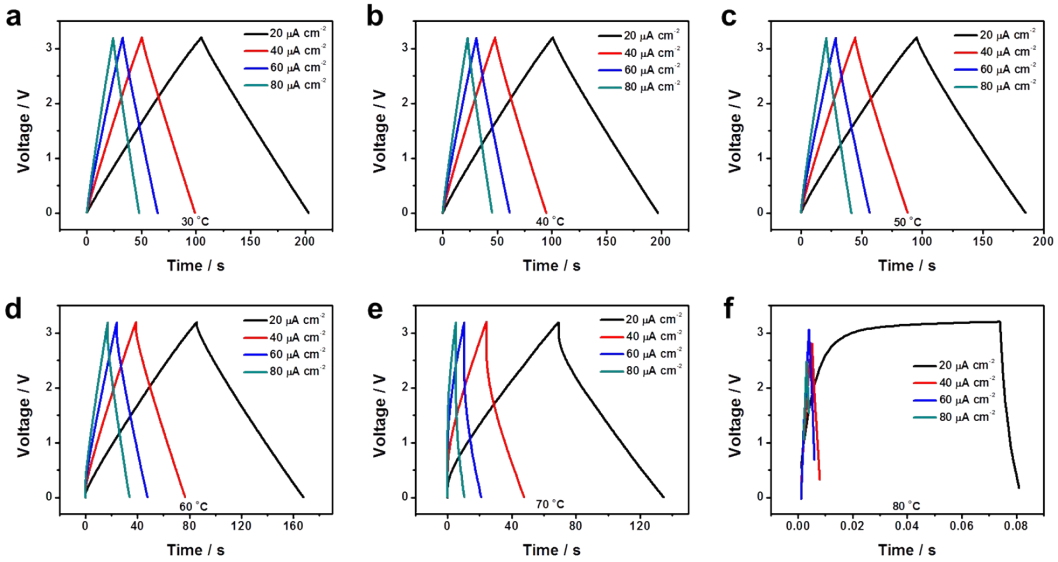

Fig. S33 GCD curves of four TS-MSCs connected in series at different current densities varied from 20 to 80 μA cm^{-2} in the temperature range of 30–80 °C.

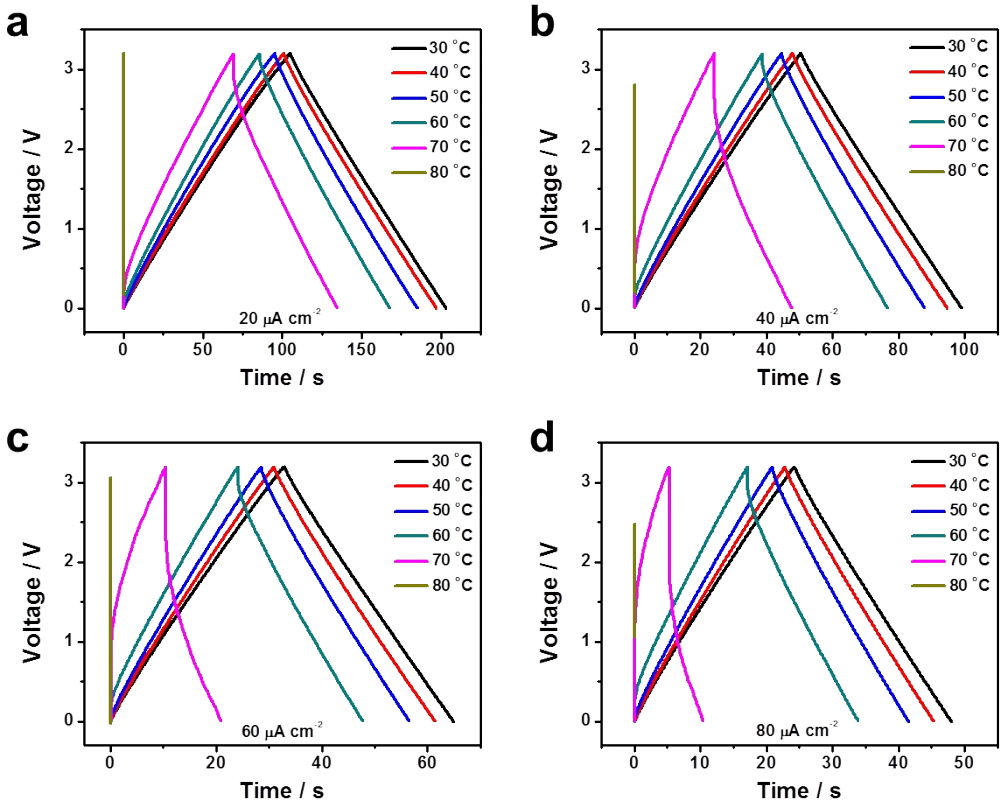

Fig. S34 Comparisons of GCD curves of four TS-MSCs connected in series at different current densities varied from 20 to 80 μA cm^{-2} in the temperature range of 30–80 °C.

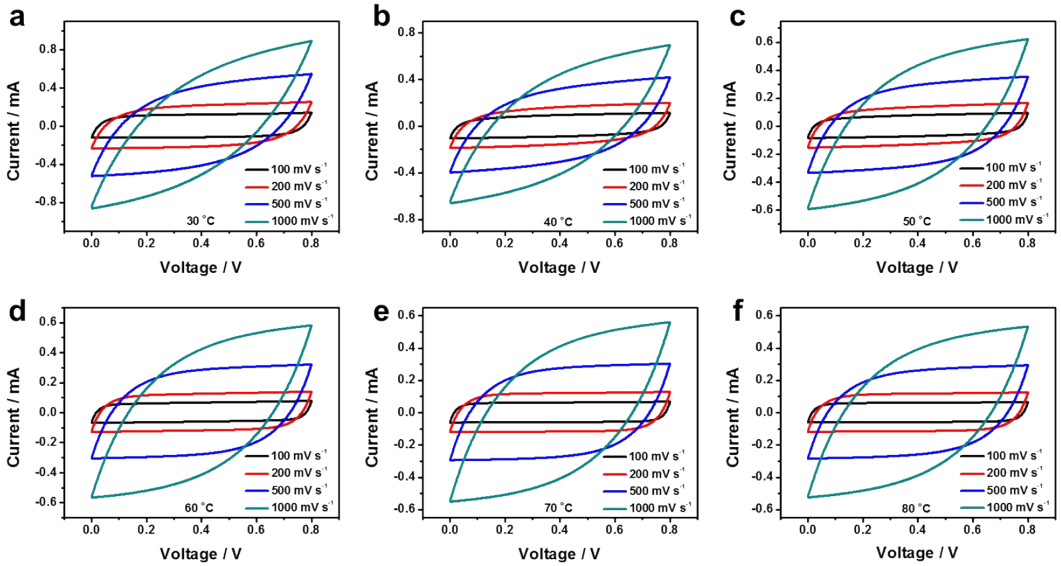

Fig. S35 CV curves of four TS-MSCs connected in parallel at different scan rates varied from 100 to 1000 mV s^{-1} in the temperature range of 30–80 °C.

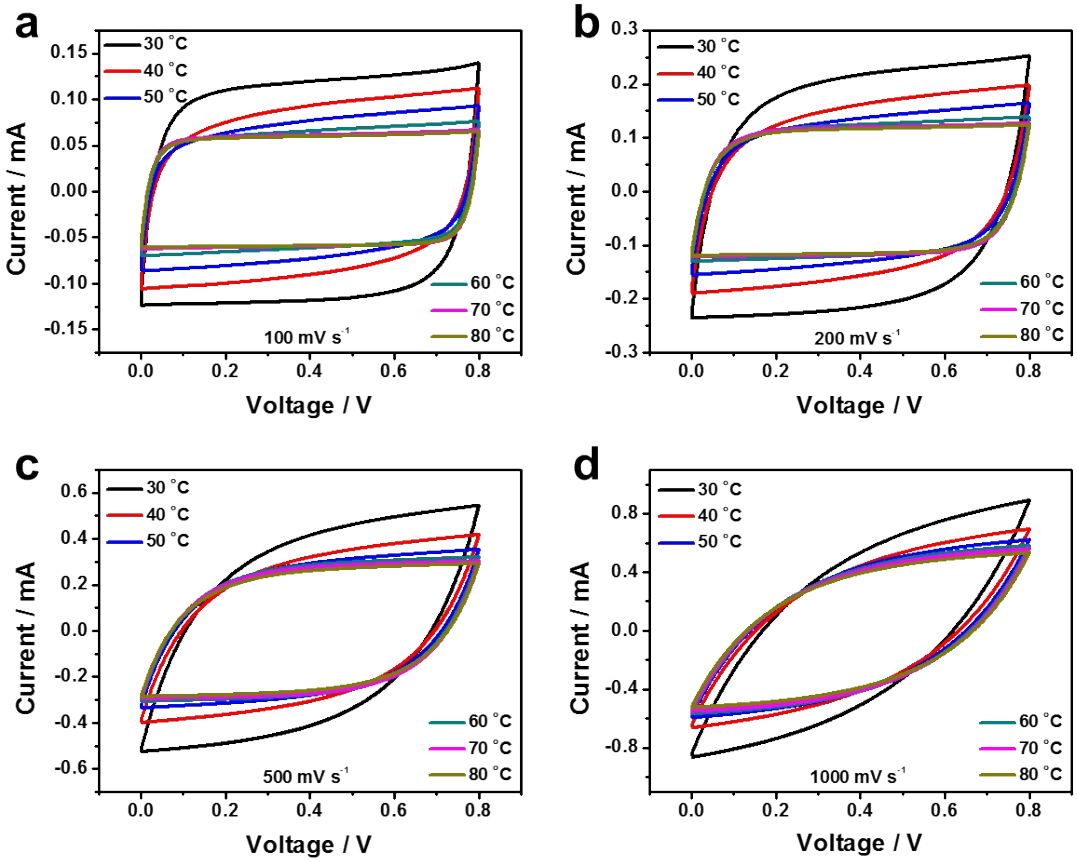

Fig. S36 Comparisons of CV curves of four TS-MSCs connected in parallel at different scan rates varied from 100 to 1000 mV s^{-1} in the temperature range of 30–80 °C.

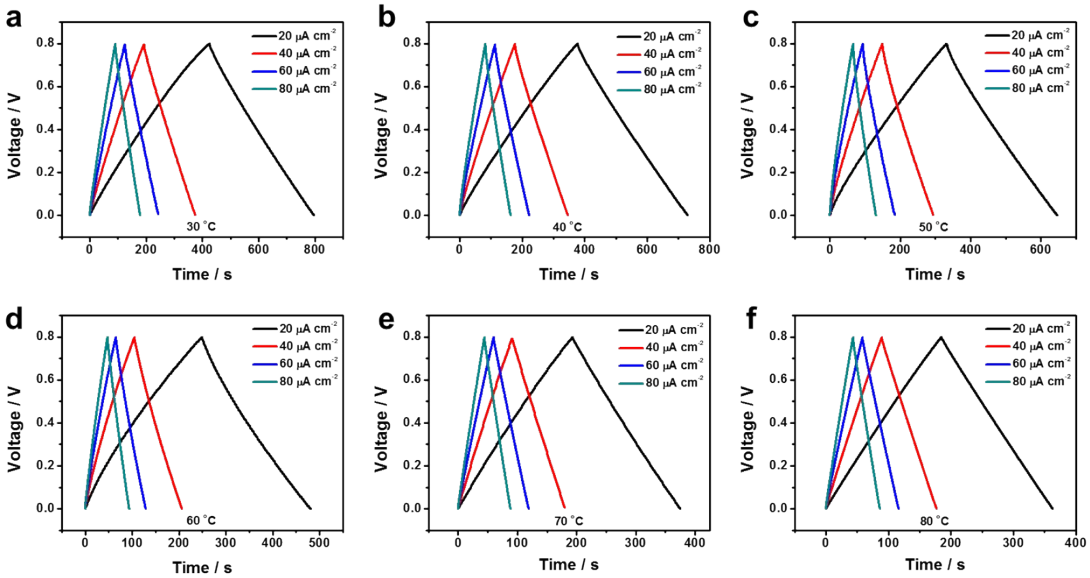

Fig. S37 GCD curves of four TS-MSCs connected in parallel at different current densities varied from 20 to 80 μA cm^{-2} in the temperature range of 30–80 °C.

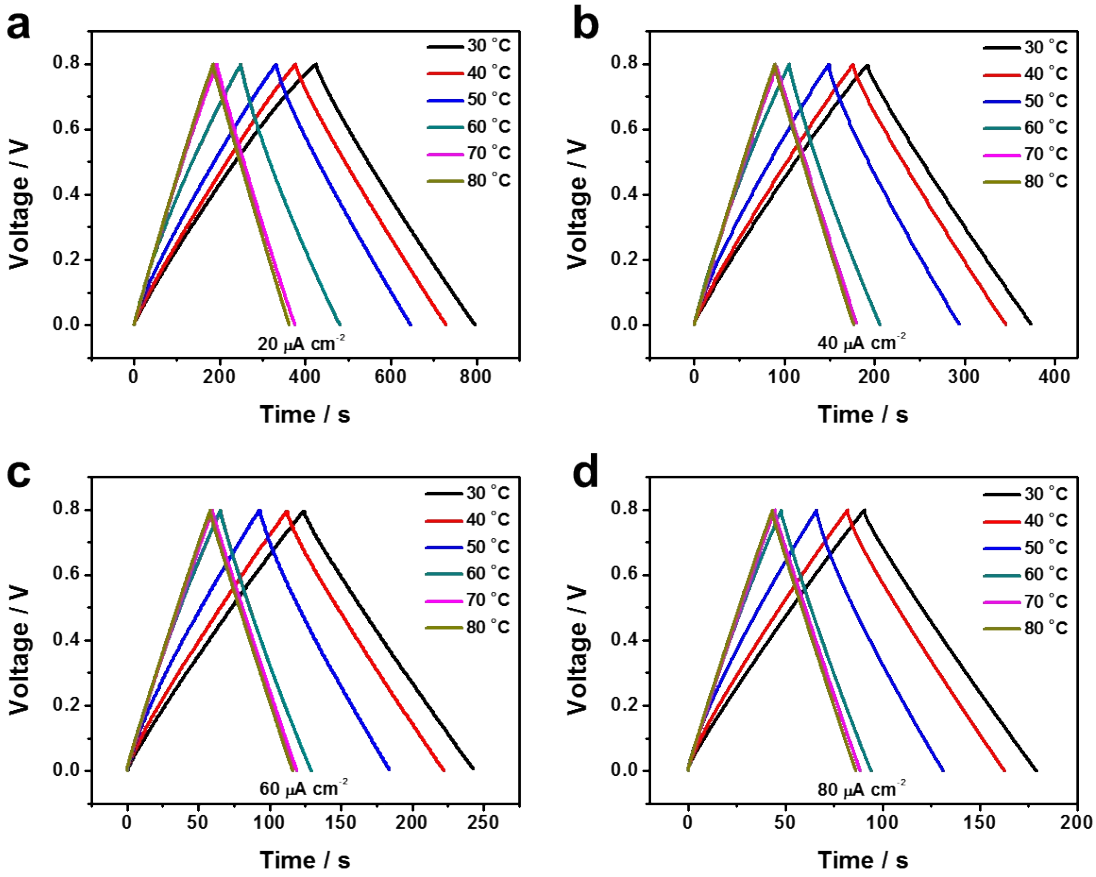

Fig. S38 Comparisons of GCD curves of four TS-MSCs connected in parallel at different current densities varied from 20 to 80 μA cm^{-2} in the temperature range of 30–80 °C.

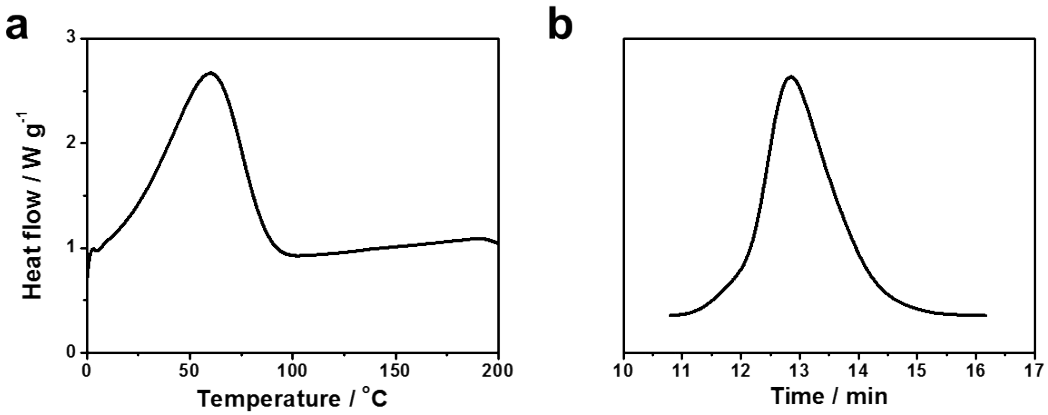

Fig. S39 Characterizations of thermo-responsive graft copolymer (PNIPAAm/MC). (a) DSC heating thermogram. (b) GPC curve.

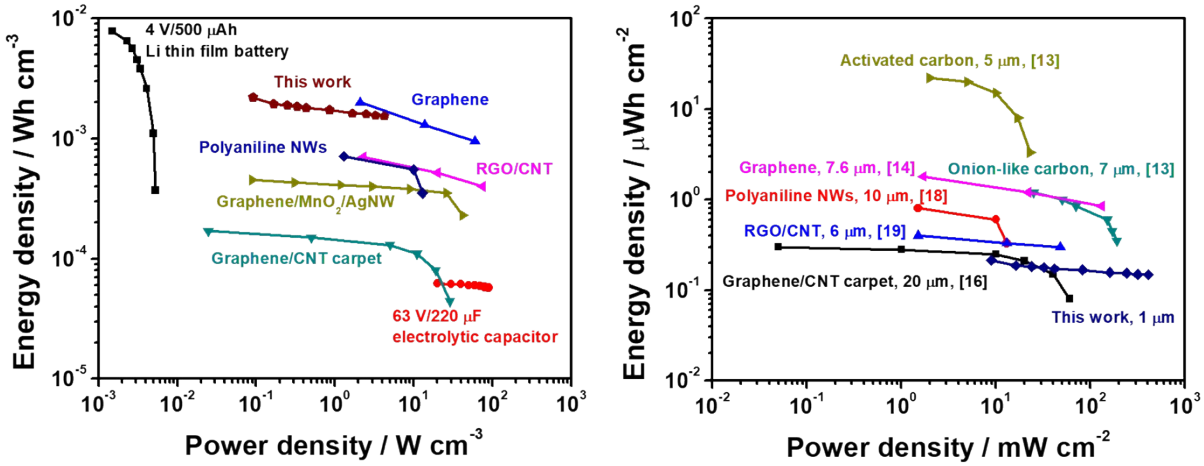

Fig. S40 Ragone plots for TS-MSC, reported Li thin film battery, activated carbon-based electrolytic capacitor, graphene-based MSCs and conducting polymer-based MSCs. Left: volumetric performance; Right: areal performance.

Table S1 Electrochemical performance of in-plane MSCs.

Electrode material	Film thickness	Electrolyte, voltage window, scan rate	Specific capacitance		Ref.
			Areal (mF/cm^2)	Volumetric (F/cm^3)	
Carbon onions	7 μm	$TEABF_4$/PC, 0-3.0 V, 1 V/s	1.7	1.35	13
Graphene	7.6 μm	PVA/H_2SO_4, 0-1.0 V, 6.8 mA/cm^3	2.32	3.05	14
Graphene	15 nm	PVA/H_2SO_4, 0-1.0 V, 10 mV/s	0.08	17.9	15
Graphene-CNT carpet	20 μm	1.0 M Na_2SO_4, 0-1.0 V, 1 A/cm^3	2.16	1.08	16
RGO/MnO_2/AgNW hybrid film	60 nm	0.5 M Na_2SO_4, 0-0.9 V, 10 mV/s	-	4.42	17
Electrochemically polymerized PEDOT	1 μm	PNIPAAm/MC/LiCl, 0-0.8 V, 100 mV/s	2.4	25	This work

Performance evaluation

According to these GCD curves at different current densities, the areal and volumetric capacitances (C_A and C_V) at room temperature were calculated (Fig. S12d) to be 2.4 mF cm^{-2} and 25 ± 5 F cm^{-3} at a current density of 20 μA cm^{-2}, respectively, both of which are superior to those of reported MSCs, such as carbon onions-MSC (C_A: 1.7 mF cm^{-2}; C_V: 1.35 F cm^{-3}),[13] graphene-MSC (C_A: 0.08 mF cm^{-2}; C_V: 17.9 F cm^{-3}),[15] graphene-carbon nanotube (CNT) carpet-MSC (C_A: 2.16 mF cm^{-2}; C_V: 1.08 F cm^{-3}),[16] graphene-MSC (C_A: 2.32 mF cm^{-2}; C_V: 3.05 F cm^{-3}),[14] and graphene/MnO_2/Ag nanowire (NW)-MSC (C_V: 4.42 F cm^{-3})[17] (Table S1).

To demonstrate the performances of TS-MSC at room temperature, Ragone plots are shown in Fig. S40. Remarkably, the single TS-MSCs deliver the volumetric energy densities of 2.3 mWh cm^{-3} (power density of 92 mW cm^{-3}) in the thermoresponsive electrolyte, which are comparable to or higher than those of recently reported MSCs based on other materials, including laser-scribed graphene,[14] graphene-CNT carpet,[16] polyaniline nanowires (NW),[18] reduced graphene oxide and carbon nanotube composites,[19] and graphene/MnO_2/Ag NW.[17] The energy density value is about two orders of magnitude higher than those of commercial electrolytic capacitors (63 V/220 μF), and even comparable to those of the thin-film lithium battery (4 V/500 μAh). The above results demonstrate that the TS-MSCs have excellent electrochemical performances with simultaneously high volumetric energy density and power density.

Reference:

1 W. Liu, B. Zhang, W. W. Lu, X. Li, D. Zhu, K. D. Yao, Q. Wang, C. Zhao and C. Wang, *Biomaterials*, 2004, **25**, 3005.
2 P. Subramanian, N. Clark, B. Winther-Jensen, D. MacFarlane and L. Spiccia, *Aust. J. Chem.*, 2009, **62**, 133.
3 B. Winther-Jensen and K. West, *Macromolecules*, 2004, **37**, 4538.
4 N. Kurra, M. K. Hota and H. N. Alshareef, *Nano Energy*, 2015, **13**, 500.
5 Q. Jiang, N. Kurra and H. N. Alshareef, *Adv. Funct. Mater.*, 2015, **25**, 4976.
6 X. Zhao, M. Dong, J. Zhang, Y. Li and Q. Zhang, *Nanotechnology*, 2016, **27**, 385705.
7 S. Marciniak, X. Crispin, K. Uvdal, M. Trzcinski, J. Birgerson, L. Groenendaal, F. Louwet and W. R. Salaneck, *Synth. Met.*, 2004, **141**, 67.
8 B. Anothumakkool, R. Soni, S. N. Bhange and S. Kurungot, *Energy Environ. Sci.*, 2015, **8**, 1339.
9 D. Yuan, B. Li, J. Cheng, Q. Guan, Z. Wang, W. Ni, C. Li, H. Liu and B. Wang, *J. Mater. Chem. A*, 2016, **4**, 11616.
10 L. Fan, N. Zhang and K. Sun, *Chem. Commun.*, 2014, **50**, 6789.
11 T. M. Higgins and J. N. Coleman, *ACS Appl. Mater. Interfaces*, 2015, **7**, 16495.
12 C. Zhang, T. M. Higgins, S. H. Park, S. E. O'Brien, D. Long, J. N. Coleman and V. Nicolosi, *Nano Energy*, 2016, **28**, 495.
13 D. Pech, M. Brunet, H. Durou, P. Huang, V. Mochalin, Y. Gogotsi, P.-L. Taberna and P. Simon, *Nat. Nanotechnol.*, 2010, **5**, 651.
14 M. F. El-Kady and R. B. Kaner, *Nat. Commun.*, 2013, **4**, 1475.
15 Z. S. Wu, K. Parvez, X. Feng and K. Müllen, *Nat. Commun.*, 2013, **4**, 2487.
16 J. Lin, C. Zhang, Z. Yan, Y. Zhu, Z. Peng, R. H. Hauge, D. Natelson and J. M. Tour, *Nano Lett.*, 2013, **13**, 72.
17 W. Liu, C. Lu, X. Wang, R. Y. Tay and B. K. Tay, *ACS Nano*, 2015, **9**, 1528.
18 C. Meng, J. Maeng, S. W. M. John and P. P. Irazoqui, *Adv. Energy Mater.*, 2014, **4**, 1301269.
19 M. Beidaghi and C. Wang, *Adv. Funct. Mater.*, 2012, **22**, 4501.